

Topological structure of the entanglement radius of Yang-Mills flux tubes

Rocco Amorosso,^{a,*} Sergey Syritsyn^a and Raju Venugopalan^{b,c,d}

^a*Department of Physics and Astronomy, Stony Brook University, Stony Brook, New York 11794, USA*

^b*Physics Department, Brookhaven National Laboratory, Upton, NY 11973, USA*

^c*CFNS, Department of Physics and Astronomy, Stony Brook University, Stony Brook, NY 11794, USA*

^d*Higgs Center for Theoretical Physics, The University of Edinburgh, Edinburgh, EH9 3FD, Scotland, UK*

*E-mail: rocco.amorosso@stonybrook.edu, sergey.syritsyn@stonybrook.edu,
raju.venugopalan@stonybrook.edu*

We expand on recent work [1] demonstrating the existence of a novel entanglement radius ξ_0 characterizing flux tube entanglement entropy (FTE²) in (2+1)D Yang-Mills theory. This physical scale corresponds to the intrinsic thickness of the flux tube that must be fully severed by an entangling region for color degrees of freedom in the flux tube to contribute non-zero FTE². We consider here geometries of the entanglement region V on the lattice where the length of the region cross-cutting the flux tube is of the same magnitude as ξ_0 . Our results further the conclusions of [1] by adding detailed new information on the topological structure of the entanglement radius of color flux tubes.

*The 42nd International Symposium on Lattice Field Theory (LATTICE2025)
2-8 November 2025
Tata Institute of Fundamental Research, Mumbai, India*

*Speaker

1. Introduction

Entanglement entropy is a powerful tool for understanding quantum gauge theories, revealing how information is distributed across their constituent parts. A standard measure of entanglement is the von Neumann entanglement entropy, with

$$S^{\text{EE}} = -\text{Tr}(\hat{\rho}_V \log \hat{\rho}_V), \quad (1)$$

where $\hat{\rho}_V$ is the reduced density matrix, defined as

$$\hat{\rho}_V = \text{Tr}_{\bar{V}} \hat{\rho}. \quad (2)$$

Calculating the von Neumann entanglement entropy on the lattice is not feasible. One instead typically takes advantage of the replica trick, calculating the Rényi entropy of order q ,

$$S^{(q)} = \frac{1}{1-q} \log(\text{Tr} \hat{\rho}_V^q), \quad (3)$$

which can be calculated using a q -replica lattice, with q an integer greater than or equal to two. The Rényi entropy has been used to calculate the entanglement entropy on the lattice in many recent studies [2–10].

However, in order to calculate the entanglement entropy in gauge theories, there are multiple well-known problems that must be addressed. Firstly, the Hilbert space of gauge invariant states cannot be factorized into gauge invariant subspaces. As the definition of the Rényi entanglement entropy relies on a partial trace, one needs a more rigorous definition of the reduced density matrix that addresses the issue of gauge invariance. This problem has been addressed extensively in the literature, with algebraic and extended lattice constructions providing gauge-invariant definitions of $\hat{\rho}_V$. These have been implemented in lattice calculations of the entanglement entropy using the replica method [3, 11–16].

Another significant issue is that the entanglement entropy in gauge field theories is typically divergent in the UV-limit, scaling with the area for $D > 2$ [17, 18]. As a result, lattice studies have mainly focused on associated quantities with a finite continuum limit, an example being the entropic C-function [2, 3, 19], which is proportional to the derivative of the entanglement entropy with respect to an infrared regulator.

In previous work, we defined a novel flux tube entanglement entropy (FTE²) [1, 20–23], defined as the excess entanglement entropy of a region of gluon fields that can be attributed to the presence of a quark-antiquark pair and associated flux tube in pure gauge Yang-Mills theory. In [21, 22], we showed that FTE² is finite and gauge invariant. In [1, 23], we extended these studies, demonstrating that FTE² is a powerful probe of the internal structure of the flux tube. In particular, we uncovered a novel physical scale of the theory, the entanglement radius ξ_0 , an effective intrinsic thickness of the vibrating color flux tube. In this work, we further explore FTE², studying the FTE² of regions with linear size $L_x \sim \xi_0$, investigating the entangling dynamics of the color flux tube when the entangling region has length on the scale of the flux tube's internal structure.

2. Flux Tube Entanglement Entropy (FTE²) review

In this section, we give an overview of past results regarding flux tube entanglement entropy, beginning with how it is calculated on the lattice and ending with a brief discussion of its relation to the internal structure of the color flux tube. For a more detailed review of FTE² in (2+1)D and (1+1)D, we refer the readers to Refs. [21, 22]. For detailed expositions of FTE²'s relevance to the internal structure of the color flux tube in (2+1)D, we refer the readers to Refs. [1, 23].

In quantum field theory, the entanglement entropy S generally takes form [2, 24–27]

$$S = S_{UV} + S_f, \quad (4)$$

where S_{UV} and S_f are the UV-divergent and finite components of the entanglement entropy, respectively. As noted, to extract information about S_f , one can study the entropic C-function. In the presence of a static quark pair, FTE² represents an alternative method of isolating S_f . FTE² is defined as [22]

$$\tilde{S}_{|Q\bar{Q}}^{(q)} \equiv S_{|Q\bar{Q}}^{(q)} - S^{(q)}, \quad (5)$$

with $S_{|Q\bar{Q}}$ representing the entanglement entropy in the presence of static quarks and S representing the entanglement entropy of the vacuum. The superscript (q) denotes the Rényi entropy of order q , typically set to $q = 2$. FTE² isolates the finite portion of the entanglement entropy by subtracting the UV-divergent vacuum entanglement, leaving a finite component that can be attributed to the flux tube. This subtraction was demonstrated to give a finite continuum limit in (1+1)-dimensions [21] for all gauge groups and for (2+1)-dimensions [22, 23] for gauge groups SU(2) and SU(3).

2.1 FTE² on the lattice

To calculate FTE² on the lattice, one utilizes Polyakov loops and the replica trick. For a detailed explanation of the lattice structure involved, we refer the reader to Ref. [22]. We follow the procedure of Refs. [4, 5, 28] to generate $\hat{\rho}_V^q$, stacking q independent replicas, each of size $L_\tau = \beta = T^{-1}$ in the temporal direction. The resulting lattice has two regions: region V and its complement \bar{V} , each with a different temporal periodicity. In region V , gauge links from adjacent replicas, representing in- and out-states of $\hat{\rho}_V$, are identified, resulting in a long periodic time extent qL_τ . Explicitly, for gauge links U oriented in spatial direction $\hat{\mu}$, we identify $U_{\hat{\mu}}(\tau = \beta)^{(r)} = U_{\hat{\mu}}(\tau = 0)^{(r+1)}$ for $r < q$ and $U_{\hat{\mu}}(\tau = \beta)^{(q)} = U_{\hat{\mu}}(\tau = 0)^{(1)}$, where superscript (r) denotes the replica number. In region \bar{V} , gauge links within the same replica at $\tau = 0$ and $\tau = \beta$ are identified, representing the in- and out-states of $\hat{\rho}$ in \bar{V} , which must be traced over to give the reduced density matrix of region V . Explicitly, $U_{\hat{\mu}}(\tau = 0)^{(r)} = U_{\hat{\mu}}(\tau = \beta)^{(r)}$ for each replica r , resulting in normal periodic time extent L_τ . This geometry is illustrated in (1+1)-dimensions in Fig. 1.

Quark and antiquark sources, represented by temporal Polyakov loops on the lattice, are placed in \bar{V} , resulting in $2q$ Polyakov loops of length L_τ . FTE² can be calculated from the correlation of these $2q$ Polyakov loops [20, 22],

$$\tilde{S}_{|Q\bar{Q}}^{(q)} \equiv S_{|Q\bar{Q}}^{(q)} - S^{(q)} = -\frac{1}{q-1} \left(\ln \frac{Z_{|Q\bar{Q}}^{(q)}}{Z_{|Q\bar{Q}}^q} - \ln \frac{Z^{(q)}}{Z^q} \right) = -\frac{1}{q-1} \ln \left(\frac{\langle \prod_{r=1}^q \text{Tr} P_{\vec{x}}^{(r)} \text{Tr} P_{\vec{y}}^{(r)\dagger} \rangle}{(\langle \text{Tr} P_{\vec{x}} \text{Tr} P_{\vec{y}}^\dagger \rangle)^q} \right). \quad (6)$$

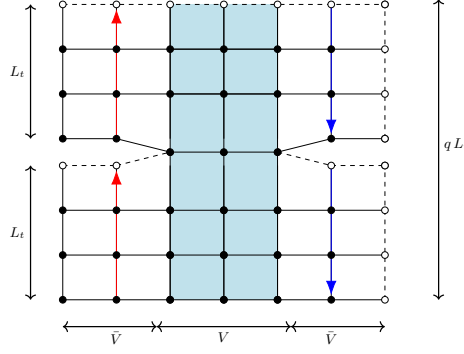


Figure 1: Correlator of Polyakov loops representing quark (red) and antiquark (dark blue) sources in a $q = 2$ replica $L_s \times L_\tau = 6 \times 3$ lattice with region V (shaded blue) having length $L_x = 2a$. The lattice has periodicity L_s in the spatial direction. The lattice is L_τ -periodic in region \bar{V} and $2L_\tau$ -periodic in region V . Dashed gauge links and open vertices are images, respectively, of solid gauge links and filled vertices, determined by the respective temporal or spatial periodic boundary conditions.

where $\text{Tr} P_{\vec{x}}^{(r)}$ is the trace of the Polyakov loop at location \vec{x} in replica r , while $\text{Tr} P_{\vec{x}}$ is the trace of the Polyakov loop in the standard one-replica lattice.

2.2 Previous results

FTE² has been studied in detail in both (1+1) and (2+1) dimensions. The (2+1)D studies of FTE² have primarily utilized the “half-slab” geometry depicted in Fig. 2(left), where both the quark and the antiquark were placed in region \bar{V} and separated by a distance L . Through studying the half-slab geometry, FTE² was found to split into two components

$$\tilde{S}_{|Q\bar{Q}}^{(q)} = S_{\text{internal}} + S_{\text{vibrational}}, \quad (7)$$

where S_{internal} represents the entanglement entropy due to color degrees of freedom within the flux tube, while $S_{\text{vibrational}}$ represents the entanglement due to mechanical vibrations of the flux tube. In this work, we focus primarily on the internal entropy, which dominates $\tilde{S}_{|Q\bar{Q}}^{(q)}$ at the quark separations studied here ($0.67 < L\sqrt{\sigma_0} < 0.89$), and is known to make up $\sim 95\%$ of FTE² [22].¹

Motivated by the results of FTE² in (1+1)D, S_{internal} was conjectured to take form [21, 22]

$$S_{\text{internal}} = \langle F \rangle \cdot \log(N_c), \quad (8)$$

where $\langle F \rangle$ is the average number of times the flux tube crosses the V/\bar{V} spatial boundary. We obtain results for (2+1)D SU(2) Yang-Mills consistent with this expectation [22]. When region V is placed between the quark pair, forcing the flux tube between them to cross region V , then $\tilde{S}_{|Q\bar{Q}} \sim 2 \ln(2)$ due to crossing the V/\bar{V} boundary twice. When the entangling region was moved far from the quark pair, $\tilde{S}_{|Q\bar{Q}} \sim 0$, as it is energetically unfavorable for the flux tube to deflect long distances and cross into region V . Moving the slab V such that it only partially separates quark and antiquark produced an interpolation between these two limits consistent with Gaussian deflection of the effective string.

¹ $S_{\text{vibrational}}$ scales $\propto \frac{1}{4} \log(L)$ at $q = 2$. Therefore, for sufficiently long quark separations, the vibrational entanglement entropy will be the dominant contribution.

This study was extended to different values of N_c and regions V composed of multiple disconnected subregions (allowing $F > 2$) in Ref. [23], finding agreement with the $\langle F \rangle \ln N_c$ with small but significant deviations. By studying multi-slab geometries, these deviations are understood to be caused by a small finite thickness of the vibrating flux tube. In [1, 23], the FTE^2 of a region V consisting of two disconnected subregions was studied as a function of the distance between the two subregions. FTE^2 varies smoothly as a function of the separation before jumping sharply as the two subregions are brought into contact. This result is incompatible with a zero-width effective string. It instead is compatible with a thick vibrating effective string that must be *fully severed* in order to contribute $F \ln N_c$ to FTE^2 . This novel model of a vibrating effective string was studied using multiple geometries of region V in [1], giving a consistent value of the effective thickness of the flux tube. This physical quantity, which we call “entanglement radius”, has the value $\xi_0 = 0.185(6)\sigma_0^{-1/2}$, where σ_0 is the string tension at zero temperature.

This entanglement radius is related to another scale of the flux tube’s internal structure, the intrinsic width [29, 30]. Taking the derivative of FTE^2 with respect to the displacement x of the entangling region from the quark-antiquark pair line, $\partial_x \tilde{S}_{|Q\bar{Q}}$ was found to have a Gaussian peak centered at $x = -\xi_0$ and exponential decay $\propto e^{-x/\lambda}$ in its tails – this decay length $\lambda\sqrt{\sigma_0} = 0.223(15)$ is consistent with both the inverse glueball mass [31] and the intrinsic width of the flux tube [30]. This deviation from Gaussianity due to the intrinsic width suggests that the entanglement radius is not fixed at one value, but instead follows a distribution. In [1], it was proposed that the entanglement radius arises from a distribution $P(\xi)$ with mean ξ_0 and support over a broad range of values ξ . In this work, we explicitly test this proposal, studying regions V with length $L_x \sim \xi_0$.

3. Results for small-slab geometry

We present here calculations further exploring the structure of FTE^2 for $SU(2)$ Yang-Mills gauge theory on a (2+1)D lattice. We utilize the standard Wilson plaquette Yang-Mills action, performing Monte Carlo sweeps with details identical to those of [22] on a $128 \times 256 \times 64$ lattice. Simulations are performed at $T_c/4$ and lattice coupling $\beta = 24.744$, consistent with lattice spacing $a\sqrt{\sigma_0} = 0.0557(11)$. FTE^2 values were obtained for the “small-slab” geometry configuration shown in Fig. 2(right), with slab length $L_x \sim \xi_0$ and width $w = 4a$. The interpretation of these results depends strongly on the observation in [1, 23] that FTE^2 behaves topologically, such that the flux tube has to be *completely severed by entangling region V*, crossing the boundary with its full width, in order to contribute to FTE^2 . Fig. 3 illustrates flux tube configurations that overlap with region V to create both full and partial boundary crossings.

We begin by studying the x -dependence of FTE^2 . The x -dependence of FTE^2 with a quark separation of $L\sqrt{\sigma_0} = 0.67$ is shown in Fig. 4. FTE^2 has a roughly Gaussian form as a function of x , in line with expectations of a thick effective string exhibiting Gaussian deflection with $L_x \sim \xi_0$. We expect the mean square transverse deflection of the flux tube to grow logarithmically [32] as the quark-antiquark separation is increased, resulting in a wider FTE^2 profile with a less-pronounced peak. The dependence of FTE^2 on the quark-pair separation L is shown in Fig. 5(left). As expected, the Gaussian peak becomes significantly smaller and wider as the quark separation increases. While we expect larger quark separations to produce a profile with higher tails, we lack statistical precision to resolve such features in sufficient detail.

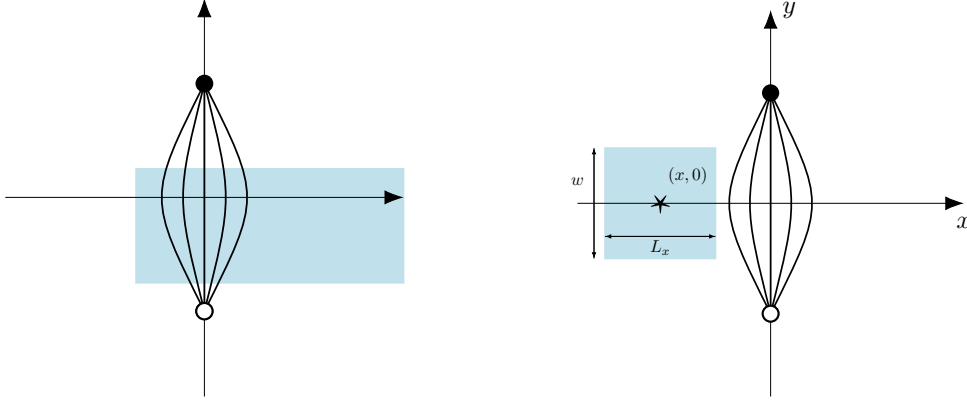


Figure 2: (Left) A depiction of the “half-slab” geometry of Ref. [22], with region V (shaded blue) having length L_x equal to half of the x -extent of the lattice. (Right) A depiction of the “small-slab” geometry, with region V (shaded blue) of variable length L_x in the x direction. The quark and antiquark sources are separated by distance L and located at $(0, \pm L/2)$.

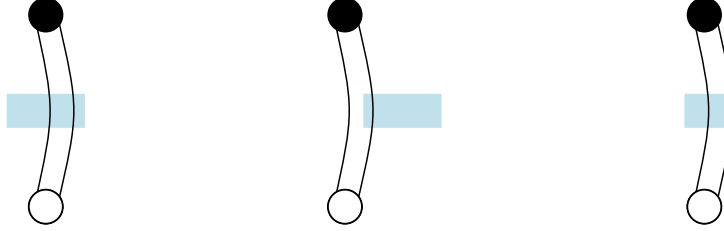


Figure 3: Examples of different overlaps of the flux tube with the entangling region V (shaded blue). (Left) The flux tube exhibits a full boundary crossing and contributes $2 \ln 2$ to FTE^2 . (Center) The center of the slab V is too far to the right (x too large) to fully sever the flux tube; the flux tube exhibits a partial boundary crossing and does not contribute to FTE^2 . (Right) The length (L_x) of the slab V is too small relative to ξ_0 ; the flux tube exhibits a partial boundary crossing and does not contribute to FTE^2 .

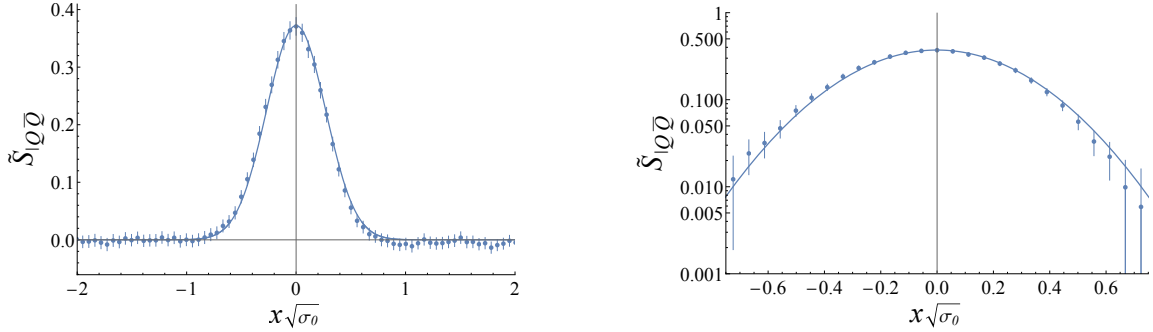


Figure 4: Dependence of $\text{FTE}^2 \tilde{S}_{|Q\bar{Q}}$ on the transverse position of the slab x computed with small-slab geometry (Fig. 2), in linear (left) and logarithmic (right) scale. Calculations are done in (2+1)D $SU(2)$ Yang-Mills theory with $Q\bar{Q}$ distance fixed to $L\sqrt{\sigma_0} \approx 0.67$. The solid line shows the fit to a Gaussian shape.

We expect FTE^2 to grow as a function of L_x . Comparing Fig. 3 left and right, qualitatively, the shorter slab is less likely to exhibit a full boundary crossing than a longer slab. To quantify these remarks, consider a region V centered at x with length L_x . Also consider an effective string

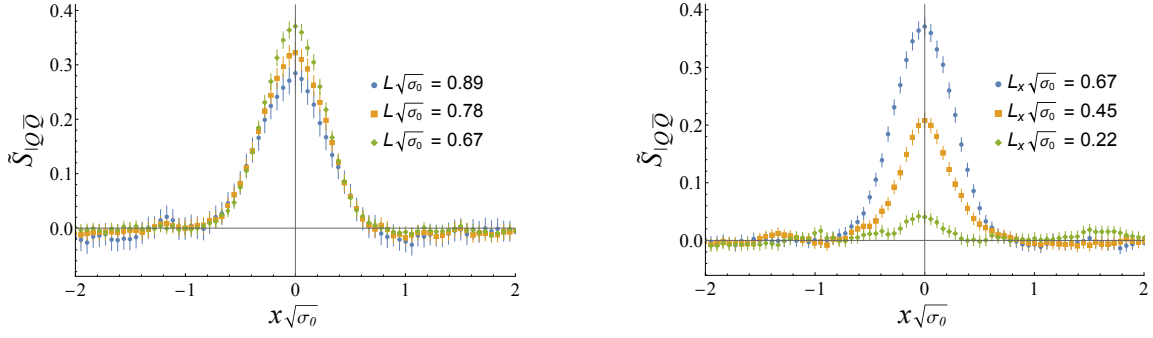


Figure 5: (Left) Plot of FTE^2 as a function of x with varying values of the quark separation L . Note that the FTE^2 value of the peak of each profile decreases as L increases. (Right) FTE^2 as a function of x with varying values of the slab length L_x . The FTE^2 value of the peak of each profile increases significantly as L_x increases. At the other extreme $L_x\sqrt{\sigma_0} = 0.22$, the FTE^2 contribution at $x = 0$ is still non-zero despite $L_x < 2\xi_0 \sim 0.37\sigma_0^{-1/2}$.

representing the flux tube with entanglement radius ξ . The center of the effective string deflects to point $(\chi, 0)$, with its leftmost and rightmost walls being at $\chi_L = \chi - \xi$ and $\chi_R = \chi + \xi$ respectively. The flux tube, and region V , exhibit a full boundary crossing when the entirety of the flux tube is in V . This is equivalent to satisfying both conditions $(x - L_x/2) < \chi_L$, $\chi_R < (x + L_x/2)$. Increasing L_x relaxes these bounds, allowing flux tubes with a wider range of deflections χ to contribute FTE^2 as well. We do in fact observe this expected behavior, with FTE^2 strongly depending on L_x . The results of this study can be seen in Fig. 5(right).

The L_x -dependence of FTE^2 allows us to probe the entanglement radius further. In Ref. [1], the average entanglement radius was found to be $\xi_0 = 0.185(6)\sigma_0^{-1/2}$. There it was also proposed that the entanglement radius of the flux tube follows some distribution $P(\xi)$. Studying the L_x -dependence of FTE^2 gives us explicit confirmation that $P(\xi)$ has support over values $\xi < \xi_0$. Indeed, we observe that FTE^2 is nonzero even for $L_x < 2\xi_0$. Specifically, at both $L_x\sqrt{\sigma_0} = 0.22$ and $L_x\sqrt{\sigma_0} = 0.33$ we observe FTE^2 values significantly above zero despite their slab length being less than $2\xi_0\sqrt{\sigma_0} = 0.370(12)$.

Comparing the FTE^2 values at $x = 0$ for varying slab lengths, one can examine different models of flux tube entanglement. In Fig. 6, we show FTE^2 as a function of L_x alongside the expectations of three models: an effective string with zero entanglement radius, a fixed entanglement radius $\xi = \xi_0$, and an exponentially decaying distribution $P(\xi)$. One can see that the fixed entanglement radius model does not describe the data well; on the contrary, the data shows stronger agreement with the model in which the entanglement radius is allowed to follow an exponential distribution.

4. Discussion

In this work, we continued our studies of the color flux tube's internal dynamics in SU(2) (2+1)D Yang-Mills theory using flux tube entanglement entropy. By studying the FTE^2 with spatial regions having length comparable to the entanglement radius, a novel scale parameterizing the flux tube's intrinsic thickness [1], we were able to obtain preliminary results detailing the internal structure of the color flux tube. We found that FTE^2 behaves largely as expected, having a roughly

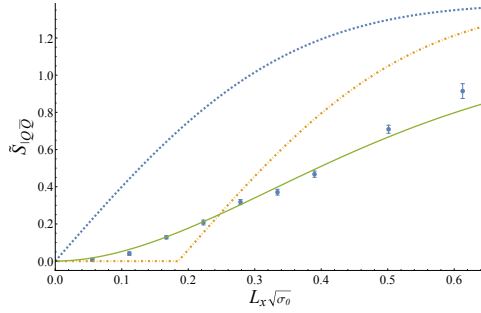


Figure 6: FTE² at $x = 0$ as a function of the slab length L_x with fixed $Q\bar{Q}$ pair separation $L\sqrt{\sigma_0} = 0.67$. The data is compared to three models of an effective string with zero entanglement radius (dashed, blue), with a fixed entanglement radius $\xi = \xi_0$ (dashed-dotted, orange), and with varying exponentially-distributed entanglement radius $\sim P(\xi)$ (solid, green). All models assume Gaussian probability for the transverse deflection of the flux tube with standard deviation $s\sqrt{\sigma_0} = 0.27$.

Gaussian form as a function of slab transverse position, decreasing as quark and antiquark are further separated, and increasing with the length of the entangling region. These preliminary results support the conclusions of Ref. [1] that the flux tube is well-modeled by an effective string with Gaussian deflection and finite non-zero entanglement radius. Our results also strongly suggest that the entanglement radius follows a distribution $P(\xi)$ with mean ξ_0 and support over a wide distribution of values ξ . In the future, we expect to increase statistical precision for our $SU(2)$ results as well as extend our studies of the small-slab geometry to larger N_c . With these additional data, we expect to make quantitative statements regarding the flux tube's internal structure and the functional form of the distribution of entanglement radii $P(\xi)$.

Acknowledgements

R.A. is supported by the Simons Foundation under Award number 994318 (Simons Collaboration on Confinement and QCD Strings). S.S. and R.A. (partially) are supported by the National Science Foundation under award PHY-2412963. In addition, R.A. is supported in part by the Office of Science, Office of Nuclear Physics, U.S. Department of Energy under Contract No. DEFG88ER41450. R.V. is supported by the U.S. Department of Energy, Office of Science under contract DE-SC0012704. R.V.'s work on quantum information science is supported by the U.S. Department of Energy, Office of Science, National Quantum Information Science Research Centers, Co-design Center for Quantum Advantage (C²QA) under contract number DE-SC0012704. R.V. was also supported at Stony Brook by the Simons Foundation as a co-PI under Award number 994318 (Simons Collaboration on Confinement and QCD Strings). R.V. acknowledges support from the Royal Society Wolfson Foundation Visiting Fellowship and the hospitality of the Higgs Center at the University of Edinburgh. The authors thank Stony Brook Research Computing and Cyberinfrastructure and the Institute for Advanced Computational Science at Stony Brook University for access to the Seawulf HPC system, which was made possible by grants from the National Science Foundation (awards 1531492 and 2215987) and matching funds from the Empire State Development's Division of Science, Technology and Innovation (NYSTAR) program (contract C210148).

References

- [1] R. Amorosso, S. Syritsyn and R. Venugopalan, *Entanglement Enabled Tomography of Flux Tubes in (2+1)D Yang-Mills Theory*, [2601.17199](#).
- [2] P.V. Buividovich and M.I. Polikarpov, *Numerical study of entanglement entropy in SU(2) lattice gauge theory*, *Nucl. Phys. B* **802** (2008) 458 [[0802.4247](#)].
- [3] P.V. Buividovich and M.I. Polikarpov, *Entanglement entropy in gauge theories and the holographic principle for electric strings*, *Phys. Lett. B* **670** (2008) 141 [[0806.3376](#)].
- [4] E. Itou, K. Nagata, Y. Nakagawa, A. Nakamura and V.I. Zakharov, *Entanglement in Four-Dimensional SU(3) Gauge Theory*, *PTEP* **2016** (2016) 061B01 [[1512.01334](#)].
- [5] A. Rabenstein, N. Bodendorfer, P. Buividovich and A. Schäfer, *Lattice study of Rényi entanglement entropy in SU(N_c) lattice Yang-Mills theory with N_c = 2, 3, 4*, *Phys. Rev. D* **100** (2019) 034504 [[1812.04279](#)].
- [6] A. Bulgarelli and M. Panero, *Entanglement entropy from non-equilibrium Monte Carlo simulations*, *JHEP* **06** (2023) 030 [[2304.03311](#)].
- [7] A. Bulgarelli and M. Panero, *Duality transformations and the entanglement entropy of gauge theories*, *JHEP* **06** (2024) 041 [[2404.01987](#)].
- [8] A. Bulgarelli, E. Cellini, K. Jansen, S. Kühn, A. Nada, S. Nakajima et al., *Flow-Based Sampling for Entanglement Entropy and the Machine Learning of Defects*, *Phys. Rev. Lett.* **134** (2025) 151601 [[2410.14466](#)].
- [9] A. Velytsky, *Entanglement entropy in SU(N) gauge theory*, *PoS LATTICE2008* (2008) 256 [[0809.4502](#)].
- [10] N. Jokela, K. Rummukainen, A. Salami, A. Pönni and T. Rindlisbacher, *Progress in the lattice evaluation of entanglement entropy of three-dimensional Yang-Mills theories and holographic bulk reconstruction*, *JHEP* **12** (2023) 137 [[2304.08949](#)].
- [11] H. Casini, M. Huerta and J.A. Rosabal, *Remarks on entanglement entropy for gauge fields*, *Phys. Rev. D* **89** (2014) 085012 [[1312.1183](#)].
- [12] S. Ghosh, R.M. Soni and S.P. Trivedi, *On The Entanglement Entropy For Gauge Theories*, *JHEP* **09** (2015) 069 [[1501.02593](#)].
- [13] W. Donnelly, *Decomposition of entanglement entropy in lattice gauge theory*, *Phys. Rev. D* **85** (2012) 085004 [[1109.0036](#)].
- [14] S. Aoki, T. Iritani, M. Nozaki, T. Numasawa, N. Shiba and H. Tasaki, *On the definition of entanglement entropy in lattice gauge theories*, *JHEP* **06** (2015) 187 [[1502.04267](#)].
- [15] R.M. Soni and S.P. Trivedi, *Aspects of Entanglement Entropy for Gauge Theories*, *JHEP* **01** (2016) 136 [[1510.07455](#)].

- [16] J. Lin and D. Radičević, *Comments on defining entanglement entropy*, *Nucl. Phys. B* **958** (2020) 115118 [1808.05939].
- [17] L. Bombelli, R.K. Koul, J. Lee and R.D. Sorkin, *A Quantum Source of Entropy for Black Holes*, *Phys. Rev. D* **34** (1986) 373.
- [18] M. Srednicki, *Entropy and area*, *Phys. Rev. Lett.* **71** (1993) 666 [hep-th/9303048].
- [19] H. Casini and M. Huerta, *A c-theorem for the entanglement entropy*, *J. Phys. A* **40** (2007) 7031 [cond-mat/0610375].
- [20] R. Amorosso and S. Syritsyn, *Entanglement Entropy due to the Presence of Static Quarks*, *PoS LATTICE2023* (2024) 382 [2311.05825].
- [21] R. Amorosso, S. Syritsyn and R. Venugopalan, *Entanglement entropy of a color flux tube in (1+1)D Yang-Mills theory*, 2411.12818.
- [22] R. Amorosso, S. Syritsyn and R. Venugopalan, *Entanglement entropy of a color flux tube in (2+1)D Yang-Mills theory*, 2410.00112.
- [23] R. Amorosso, S. Syritsyn and R. Venugopalan, *Internal color contributions to flux tube entanglement entropy*, *PoS LATTICE2024* (2025) 409 [2502.08737].
- [24] S. Ryu and T. Takayanagi, *Holographic derivation of entanglement entropy from AdS/CFT*, *Phys. Rev. Lett.* **96** (2006) 181602 [hep-th/0603001].
- [25] S. Ryu and T. Takayanagi, *Aspects of Holographic Entanglement Entropy*, *JHEP* **08** (2006) 045 [hep-th/0605073].
- [26] T. Nishioka and T. Takayanagi, *AdS Bubbles, Entropy and Closed String Tachyons*, *JHEP* **01** (2007) 090 [hep-th/0611035].
- [27] I.R. Klebanov, D. Kutasov and A. Murugan, *Entanglement as a probe of confinement*, *Nucl. Phys. B* **796** (2008) 274 [0709.2140].
- [28] P. Calabrese and J.L. Cardy, *Entanglement entropy and quantum field theory*, *J. Stat. Mech.* **0406** (2004) P06002 [hep-th/0405152].
- [29] M. Caselle and P. Grinza, *On the intrinsic width of the chromoelectric flux tube in finite temperature LGTs*, *JHEP* **11** (2012) 174 [1207.6523].
- [30] M. Caselle, E. Cellini, A. Nada, D. Panfalone and L. Verzhichelli, *Intrinsic Width of the Flux Tube as a tool to explore confining mechanisms in Lattice Gauge Theories*, 2601.19520.
- [31] M.J. Teper, *SU(N) gauge theories in (2+1)-dimensions*, *Phys. Rev. D* **59** (1999) 014512 [hep-lat/9804008].
- [32] M. Luscher, G. Munster and P. Weisz, *How Thick Are Chromoelectric Flux Tubes?*, *Nucl. Phys. B* **180** (1981) 1.